Soft Matter

Formation of Two-Dimensional Diamond-Like Colloidal Crystals Using Layer-by-Layer Electrostatic Self-Assembly

Journal:	*Soft Matter*
Manuscript ID	SM-ART-09-2023-001278.R1
Article Type:	Paper
Date Submitted by the Author:	07-Dec-2023
Complete List of Authors:	Fujita, Minori; Graduate School of Pharmaceutical Sciences, Nagoya City University Toyotama, Akiko; Nagoya City University, Okuzono, Tohru; Nagoya City University, Niinomi, Hiromasa; Tohoku University Yamanaka, Junpei; Graduate School of Pharmaceutical Sciences, Nagoya City University,

ARTICLE

Formation of Two-Dimensional Diamond-Like Colloidal Crystals Using Layer-by-Layer Electrostatic Self-Assembly

Received 00th January 20xx,
Accepted 00th January 20xx

DOI: 10.1039/x0xx00000x

Minori Fujita, [a] Akiko Toyotama, [a] Tohru Okuzono, [a] Hiromasa Niinomi [b] and Junpei Yamanaka*[a]

We report here that a two-dimensional (2D) diamond-like structure of micron-sized colloidal particles can be obtained by layer-by-layer self-assembly. Positively and negatively charged silica particles, 1 μm in diameter, were used in the experiments. On a positively charged, flat glass substrate, the first layer of negatively charged particles was prepared to form a non-close-packed 2D crystal. Then the second and third layers were fabricated using electrostatic adsorption. The positions of adsorbed particles were controllable by tuning the zeta-potential of the particles and the salt concentration of the medium. The FDTD calculations show that the 2D diamond structures of particles with higher refractive index (titania) have an absorption band in the wavelength range corresponding to the photonic band gap of the 3D bulk crystal. We expect these findings to be useful for the fabrication of novel photonic materials.

1 Introduction

A diamond lattice of colloidal particles with a structural periodicity of the wavelength of light [Fig. 1(a)] has been shown theoretically to function as a photonic crystal with a perfect three-dimensional (3D) photonic bandgap when the refractive index of the particles is sufficiently large[1]. Even an "amorphous diamond" structure that is not perfectly ordered has been reported to work as a photonic material[2], as can be seen in brightly colored bird feathers[3] etc. Single- and few-layer diamond lattices of thin GaAs nanorod arrays constructed by electron-beam lithography and micromanipulation method have been reported to have photonic band gaps[4]. Various ingenious methods have thus far been devised to fabricate colloidal diamond crystals[5-8]. Here we report a new methodology to obtain a large-area, two-dimensional (2D) diamond-like structure, which consists of a regular 2D sequence of tetrahedral clusters of particles. This structure was obtainable using electrostatic layer-by-layer particle adsorption.

Colloidal self-assembly has been actively studied[9-13]. For colloid consisting of only one kind of particle that interacts isotropically, the resulting crystals are those with high packing fractions α; the face-centred cubic (FCC, α = 74%), body-centred cubic (68%), or hexagonally close-packed (74%) crystals. On the other hand, a diamond lattice, which has a much lower α (34%), does not form spontaneously because it is entropically disfavored. Therefore, the use of binary colloids or anisotropic interactions has been studied; microscopic diamond crystals have been constructed by employing the binary systems[5,6] and DNA-modified particles[6,7] or tetrahedral particles[8].

Electrostatic interactions, which are readily tunable and long-ranged, are often significant in colloidal self-assembly. Binary colloids with opposite charges produce various kinds of alloy crystals, depending upon the size and charge ratios[14,15]. Diamond lattices of oppositely charged binary metal particles about 10 nm in diameter have been fabricated[16,17].

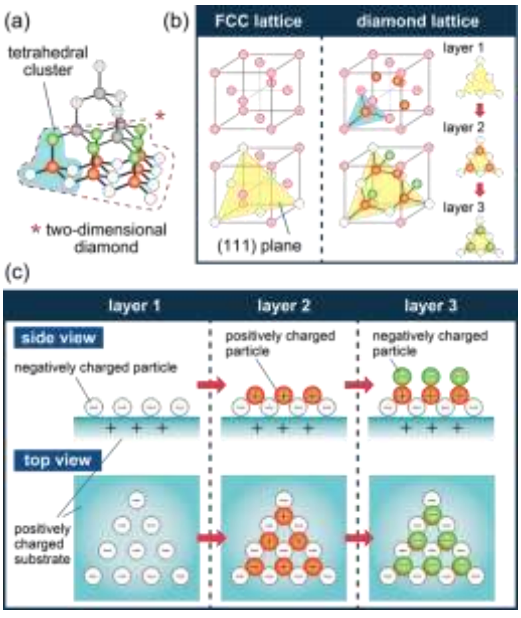

Fig. 1 (a) Diamond lattice; the region enclosed by the dashed line is the target structure of this study. (b) Comparison of the face-centred cubic (FCC) and diamond lattices. (c) The fabrication method.

The construction of a diamond lattice of micron-sized particles using electrostatic interactions has not previously been reported, although the formation of a tetrahedral

[a] Graduate School of Pharmaceutical Sciences, Nagoya City University, 3-1 Tanabe, Mizuho, Nagoya 467-8603, Japan. Email: yamanaka@phar.nagoya-cu.ac.jp
[b] Institute of Multidisciplinary Research for Advanced Materials, Tohoku University, 2-1-1 Katahira, Aoba, Sendai 980-8577, Japan
† Electronic Supplementary Information (ESI) available:
See DOI: 10.1039/x0xx00000x

cluster—which is the structural unit of the lattice—has been studied in detail[18-20]. We have recently obtained tetrahedral clusters of polystyrene and titania particles in the microgravity environment of the International Space Station[21].

Here, we propose a new method for fabricating 2D diamond structures, aiming to verify whether micron-sized charged particles form colloidal crystals with a low value of α. This method is based on our recent studies of (i) 2D-charged colloidal crystals[22], and (ii) colloidal clusters[21,23,24].

Figure 1(b) illustrates the concept of the method. The diamond lattice is "a double FCC" lattice. In Fig. 1(b) the FCC (111) plane and the corresponding plane in the diamond lattice are shown in yellow. The target structure is obtainable in the following three steps: (i) placing the particles shown in white in the FCC (111) plane as "layer 1". (ii) Arranging the "layer 2" particles (red) in the centres of the equilateral triangles of particles in "layer 1", and (iii) setting the "layer 3" particles (green) on top of the "layer 2" particles. These three layers of particles form two-dimensionally connected tetrahedral colloidal clusters, which we here call a "2D diamond structure."

To fabricate this structure, we used the layer-by-layer adsorption of charged particles illustrated in Fig. 1(c). First, a positively charged [hereafter, denoted by (+)] glass substrate was prepared and layer 1 was formed by adsorbing negatively charged [denoted by (−)] particles on it to make a triangular lattice. The (+) particles in layer 2 were next adsorbed onto the centres of the equilateral triangles of the nearest neighbours in the lattice of layer 1. The layer 3 particles again bore negative charges and were adsorbed on top of the (+) particles in layer 2. As described below, we were able to make the particles to be adsorbed in suitable positions by varying the zeta-potential ζ of the particles and/or the salt concentration C_s of the medium.

We will also discuss the optical properties of 2D diamond structures using finite difference time domain (FDTD) calculations. It is known that 3D bulk diamond crystals of high refractive index particles, for example, titania particles have a perfect photonic band gap (PBG). FDTD calculations show that 2D diamond structures constructed with titania particles have absorption bands in the wavelength region corresponding to the PBG of the 3D bulk crystal.

2 Experimental

2.1 Materials

Silica particles (Seahoster KE-P100, Nippon Catalyst Co., Ltd., Tokyo, Japan) with diameters d = 1060 nm and ζ = −46 mV (in 10 μM NaCl solution) were used as (−) particles for layers 1 and 3, which were observable by optical microscopy. (+) particles for layer 2 (d = 1120 nm, ζ = +59 mV) were synthesized by introducing a cationic polymer, polyethyleneimine (PEI), onto the (-) particles. As a substrate, we used a coverslip modified with a cationic silane coupling agent, 3-aminopropyltriethoxysilane (APTES, Shin-Etsu Chemical Co., Ltd., Tokyo, Japan), (Fig.2). Preparation of the particles and the substrate is described later in detail[22].

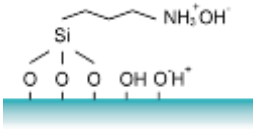

Fig. 2 Illustration of the glass substrate modified with APTES.

2.2 Preparation of the (-) particles

A powder sample of colloidal silica, KE-P100, was dispersed in Milli-Q water by ultrasonication. A mixed bed of cation- and anion-exchange resin beads (AG501-X8(D), Bio-Rad Labs., California, USA) was added to the dispersion and the sample was allowed to stand for seven days for deionization. The sample thus purified was used in the experiments as the (-) particles. We calculated the volume fraction Φ of the particles from the weight of the dried sample and the specific gravity of KE-P100 silica (= 1.90, the value determined by the manufacturer).

2.3 Synthesis of the (+) particles

Using a partially modified method of that by van Blaaderen and Vrij[25], (+) particles were synthesized in the following manner.

***(i) Preparation of RITC–APTES solution*:** 2.5 mg of rhodamine isothiocyanate (RITC, Wako Chemicals Co., Ltd., Tokyo, Japan) was dissolved in 2 mL of ethanol, sonicated, and stirred for 5 min in a Teflon container. Then 10 μL of APTES was added to the solution and the sample was stirred for 24 h. The resulting addition reaction between the isothiocyanate group of RITC and the amino group of APTES provided a reactive silane coupling agent with the rhodamine moiety, RITC–APTES.

(ii) Incorporation of RITC–APTES into silica particles: 11 mL of ethanol, 5.8 mL of Milli-Q water, 320 μL of tetraethoxysilane, and 300 μL of the RITC–APTES solution prepared in (i) were mixed, and stirred in a Teflon bottle for about 5 min. Then 840 μL of aqueous ammonia (25–27.9 mass/mass, Wako Chemicals) was added to this solution. A dispersion of 0.5 g of KE-P100 silica in 20 mL ethanol was prepared and added dropwise to it. The reaction was carried out by stirring the sample for about 20 h. Then the aqueous medium was replaced with ethanol by centrifugation.

(iii) Modification of the particle surfaces with PEI: 13 mL of ethanol, 4.3 mL of Milli-Q water, and 1.5 mL of an isopropanol solution of trimethoxysilylpropyl modified (polyethyleneimine) (Gelest Inc., Pennsylvania, USA) were stirred in a Teflon vessel for about 5 min. Next, 500 μL of 1 M HCl and 20 mL of the RITC-modified silica colloid obtained in (ii) were added to the mixture. The reaction was carried out for about 21 h. Then the sample was washed four times each with ethanol and Milli-Q water by centrifugation to substitute the medium.

(iv) Purification: The aqueous dispersion of the (+) particles thus obtained was dialyzed and purified for at least 10 days, before the experiments.

2.4 Preparation of the (+) substrate

The surface of a glass coverslip (Matsunami Co., Ltd., Tokyo, Japan) was modified with APTES to produce a positively charged substrate. We used a partially modified method of our previous one[22]. The glass coverslip was washed with ethanol, dried, and cleaned with a UV–ozone treatment for 10 min. It was then immersed in concentrated sulfuric acid for 2 h, and washed with

Milli-Q water. Thereafter, the cleaned coverslip was maintained in 0.1% APTES in 1 mM acetic acid for 1 h, rinsed with Milli-Q water, and dried. An eight-cell frame made of plastic resin was then glued to the coverslip for the experiments. The cells were treated with 0.1 M NaOH solution to hydrolyze some of the amino-group moieties introduced on the glass surface, thereby slightly reducing the number of positive charges.

Unmodified pure glass has an isoelectric point (iep) at pH ~ 2, due to the dissociation of weakly acidic silanol groups (Si–OH) on the surface. The APTES-modified glass substrate has an iep of pH ~ 8.

3 Results and Discussion

3.1 Construction of layer 1

We prepared layer 1 by our previous method[22] with some modifications. Charged colloidal particles are arranged regularly in dispersion when the electrostatic repulsion between them is sufficiently strong; this structure is referred to as a 3D charged colloidal crystal[26-28]. 2D crystal can be obtained by electrostatic adsorption of the 3D crystal onto the oppositely charged substrate. At high particle volume fraction Φ, the 3D crystal often has the FCC structure, whose (111) plane orients parallel to the substrate[22]. The 2D triangular lattice made by this procedure was used as layer 1. As illustrated in Fig. 3(a), in order to obtain a tetrahedral structure for the diamond lattice, the distance ℓ between the centres of the nearest-neighbour particles in layer 1 must be $\ell = \sqrt{(8/3)}d \sim 1.63d$. Fig. 3(b) shows that the ℓ value was tunable by Φ value of the 3D crystals. For a uniformly dispersed colloid, $\ell \sim 1.63d$ corresponds to $\Phi \sim 0.17$. However, because of the high specific gravity (~1.9) and the large size, the silica particles settled and concentrated. At Φ = 0.05, the ℓ value was 1640 ± 70 nm (averaged value and standard deviation of 200 measurements).

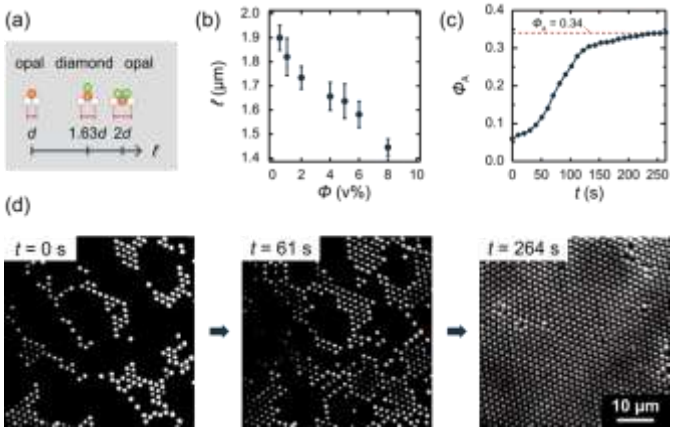

Fig. 3 (a) The nearest centre-to-centre distance ℓ between layer 1 particles with diameter d required for a diamond lattice. (b) Relationship between ℓ and the particle volume fraction Φ. (c) Time dependence of the area fraction Φ_A of the adsorbed particles. (d) Optical micrographs of the adsorption process of layer 1 particles onto the glass substrate.

We also observed adsorption process of layer 1. Figure 3(c) is the time variation of the area fraction Φ_A of the adsorbed particles. Over time, the Φ_A value asymptotically approached the ideal value of the diamond lattice, 0.34. Figure 3(d) shows snapshots taken in the course of adsorption of colloidal silica (Φ = 0.06) and these pictures were obtained from the image-analysis software, Fiji. The image recording began immediately after the sample was dropped onto the substrate (t = 0). A movie of the adsorption process is presented as ESI†.

3.2 Construction of layer 2

To form layer 2, the (+) particles need to be located in the centres of the unit triangular lattice of layer 1. Calculations of interaction potential of particles in layers 1 and 2 were carried out to examine stable structure (details are described in 3.5.1). The calculations showed that the ideal configuration for diamond lattice was energetically the most stable, irrespective of C_s. In this case, the (+) particles contacted all three neighbouring particles in the triangular lattice. However, microscopic observations showed that the (+) particles often made contact with only one or two particles in layer 1. It is likely that the strong electrostatic attraction between the (+) and (−) particles caused a substantial frictional force, preventing them from being located in the equilibrium configuration.

We therefore tuned the interaction by pH and C_s. Fig. 4(a) shows the effect of the HCl concentration, [HCl] on ζ for the (−) and (+) particles in layers 1 and 2 (blue and red symbols, respectively). For layer 1, unmodified (−) silica particles were used, whose surface charges were due to dissociation of weakly acidic silanol groups. At higher [HCl], the silanol groups were less dissociable, reducing ζ for the (−) particles, while ζ for the (+) particles did not significantly depend on [HCl]. These variations in ζ, as well as the increase in the ionic strength, appear to have resulted in the reduction of the electrostatic attraction between them at higher [HCl].

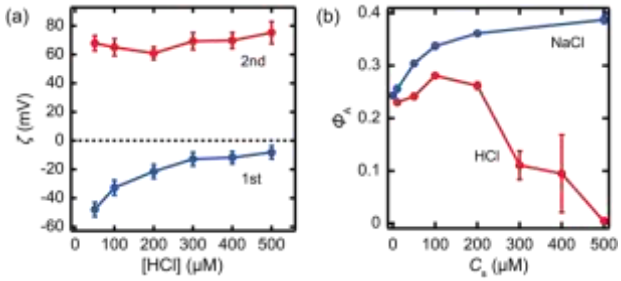

Fig. 4 (a) Variation of the zeta-potential ζ of the particles used in layers 1 and 2 with [HCl]. (b) The area fraction Φ_A of adsorbed (+) particles at varying [HCl] or [NaCl].

The adsorption amount of (+) particles onto layer 1 reflects the magnitude of interaction. We determined the [HCl] dependence of Φ_A of the (+) particles adsorbed onto layer 1 particles from micrographs [Fig. 4(b), blue symbols]. With increasing [HCl], Φ_A initially became larger and after reaching a maximum it decreased. The increase in Φ_A is because of the weakened electrostatic repulsion between adsorbed and non-adsorbed (+) particles with an increase in the ionic strength. At [HCl] = 500 μM, almost no adsorption was observed.

The variation of Φ_A upon the addition of NaCl was also examined as shown in Fig. 4(b). In this case, Φ_A increased monotonically with the NaCl concentration, [NaCl]. The ideal value of Φ_A for layer 2 (0.34) was achieved at [NaCl] ~100 μM.

Based on these results, layer 2 was prepared as follows. First, a dispersion of (+) particles with [HCl] = 500 μM was added to layer 1. Microscopic observations confirmed that the (+) particles were retained near the centres of the triangular lattice. Next, the (+) particles were adsorbed onto layer 1 by replacing the medium with an aqueous NaCl solution. We found that Φ_A ~ 0.34 was achieved when NaCl of 50–100 μM was used. After the adsorption, the excess (+) particles were removed by washing the substrate with Milli-Q water.

3.3 Construction of layer 3

Finally, layer 3 was constructed by adsorbing (−) particles near the tops of the layer 2 particles. Unlike the case for layer 2, the formation of layer 3 involves both (i) repulsion from the (−) particles in layer 1 and (ii) attraction by the (+) particles in layer 2. Interparticle potential calculations predicted that, at lower C_s, the (−) particles tended to be adsorbed on top of the layer 2 particles (discussed in 3.5.2). These experiments were performed at [NaCl] = 20 μM. After adsorption, the excess particles were removed by washing the substrate with water.

The obtained structure was observed by a confocal laser scanning microscope (LSM, type C2, Nikon, Tokyo, Japan). Beforehand, the sample was immersed in an aqueous solution of the green cationic fluorescent dye, auramine (0.5 mM), to stain the (−) particles in layers 1 and 3. Images of each layer are shown in Figs. 5(a)–5(c). A cross-section of the 3D reconstruction image is shown in Fig. 5(d). Figure 5(e) is a magnified image of Fig. 5(d). The 2D structure of connected tetrahedra can be seen clearly. Figure 5(f) shows the positions of the particles in layer 1 overlaid by those in layer 2, as obtained from image analysis of the regions represented by rectangles in Figs. 5(a)–5(c). The corresponding positional relations for the particles in layers 2 and 3 are shown in Fig. 5(g), indicating that the layer 2 particles were placed almost in the centres of the three underlying particles in layer 1, while the layer 3 particles tended to be positioned on top of the layer 2 particles.

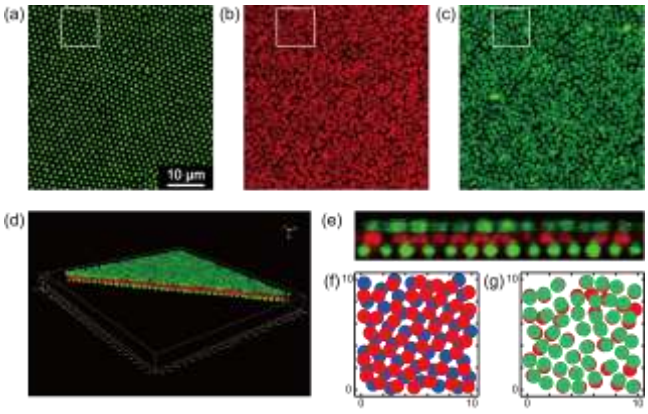

Fig. 5 Micrographs of (a) layer 1, (b) layer 2, and (c) layer 3. A scale bar in (a) applies to (b) and (c). (d) 3D reconstruction and cross-section of the structure. (e) A magnified image of the cross-section. Overlap of particles in (f) layers 1 (blue) and 2 (red), and (g) layers 2 (red) and 3 (green); size of the viewing fields = 10 × 10 μm².

3.4 Evaluation of the lattice structure

Figure 6(a) shows the radial distribution function $g(r)$ of the layer 1 particles calculated from Fig. 5(a). Here, r is the distance between particle centres. The dotted lines in Figs. 6(a) and 6(b) represent the calculated values for the FCC (111) plane with d = 1000 nm and $\ell = \sqrt{(8/3)}\, d$, which agree well with the experiments. Figure 6(b) shows $g(r)$ for layers 2 and 3 based on Figs. 5(b) and 5(c). Although their peak heights are lower than those of layer 1 because they have more structural disorder, the spatial periodicities in layers 2 and 3 are in good agreements with that of layer 1. This indicates that, on average, the particles in the three layers are arranged in a tetrahedral structure.

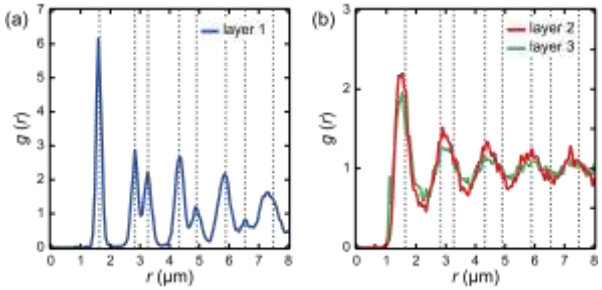

Fig. 6 Radial distribution functions for (a) layer 1 and (b) layers 2 and 3 obtained from the images in Figs. 5(a)–5(c). The dashed lines are theoretical values for the FCC (111) plane.

The regularity of the particle positions in layer 2, was evaluated in terms of the bond-orientation order parameter Ψ_3 of the particles (the equation (1)).

$$\Psi_3 = \frac{1}{3}\left|\sum_{n=1}^{3} e^{3i\theta_n}\right| \quad (1)$$

As illustrated in Fig. 7(a), the angle θ_n is the n-th (n = 1, 2, 3) bond angle of the triangular lattice of particles in layer 1; if b_n is the line passing through the n-th particle (layer 1) and the central particle (layer 2) in a micrograph, the angle between b_n and the x-axis of the coordinates is equal to θ_n. Figure 7(b) shows the Ψ_3 values at various locations of the particle in layer 2. The centre of the triangular lattice is the origin (x, y) = (0, 0), and we used a coordinate system in which the particles in layer 1 are fixed at the three points (0, 1), (-√3/2, -1/2), and (√3/2, -1/2), in an equilateral-triangular arrangement. The parameter Ψ_3 is 1 for the completely ordered structure where the particle in layer 2 is located at the centre of the equilateral triangle of the particles in layer 1, while Ψ_3 is 1/3 when the particle is on any of the sides of the equilateral triangle. A configuration with Ψ_3 = 0 exists outside the triangular lattice.

The average value of Ψ_3 was 0.85 ± 0.16 between the particles in layers 2 and 1, and 0.82 ± 0.13 for the particles in layers 3 and 1, which confirms the high regularity of the 2D-diamond-like structure.

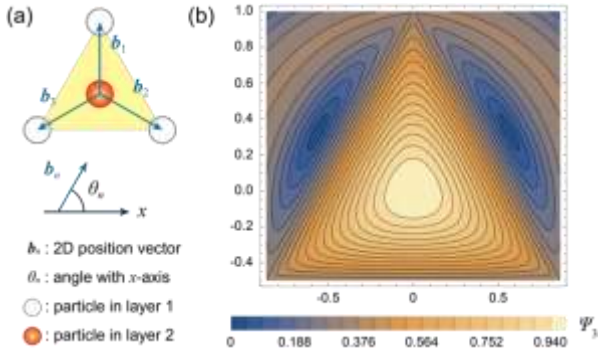

Fig. 7 (a) Definition of θ_n. (b) The parameter Ψ_3 for the layer 2 particle placed at various locations on the equilateral triangle of particles in layer 1.

3.5 Interaction between particles

3.5.1 Interaction between a (+) particle and the (–) particles in the triangular lattice of layer 1

Here, we discuss the stable position of the (+) particle in layer 2, assuming that the interaction potential $U(r)$ between two charged colloidal particles separated by a centre-to-centre distance r was expressed as the sum of the Yukawa-type electrostatic interaction potential $U_{\mathrm{Y}}(r)$ and the van der Waals potential $U_{\mathrm{vdW}}(r)$:

$$U(r) = U_{\mathrm{Y}}(r) + U_{\mathrm{vdW}}(r). \quad (2)$$

The potential $U(r)$ for particles 1 and 2 having radii a_1 and a_2, and charge numbers Z_1 and Z_2, respectively, is represented by

$$U_{\mathrm{Y}}(r) = \frac{exp[\kappa(a_1+a_2)]}{(1+\kappa a_1)(1+\kappa a_2)} \frac{Z_1 Z_2 {e_0}^2}{4\pi\varepsilon_r\varepsilon_0} \frac{exp(-\kappa r)}{r}. \quad (3)$$

Here, $1/\kappa$ is the Debye screening length, ε_r and ε_0 are the dielectric constants of the medium and vacuum, respectively, and e_0 is the elementary charge.

The potential $U_{\mathrm{vdW}}(r)$ is given by

$$U_{\mathrm{vdW}}(r) = -\frac{A}{6}\left\{\frac{2a_1a_2}{r^2-(a_1+a_2)^2} + \frac{2a_1a_2}{r^2-(a_1-a_2)^2} + ln\frac{r^2-(a_1+a_2)^2}{r^2-(a_1-a_2)^2}\right\}, \quad (4)$$

where A is the Hamaker constant between particles 1 and 2 in medium.

For calculating the interaction potential between the single (+) particle in layer 2 and the (-) particles in layer 1, contributions from seven particles in layer 1 were considered. The centre-to-centre distance between the nearest-neighbour particles in layer 1 was set to the ideal value for a diamond lattice, that is, 1.63d. The model used in the calculation is illustrated in Figs. 8(a) and 8(b). The (+) particle (shown in red) was always in contact with at least one particle in layer 1 (white). θ was defined as the angle between (1) a vertical axis and (2) a line connecting the centres of the (+) particle and the contacted particle in layer 1; θ is equal to zero when the (+) particle is on the very top of the particle in layer 1. When the (+) particle is located at the centre of an equilateral triangle of the particles in layer 1, θ has the largest value, arcsin [(2/3) √2] ~ 1.23.

We found that magnitudes of (i) the electrostatic repulsion between the (+) particle in layer 2 and the (+) charged glass substrate and (ii) the gravitational potential energy of the particle in layer 2 were negligibly small. Therefore, the sum of the interaction potential between the (+) particle and the (-) particles forming the triangular lattice in layer 1 was calculated to examine the stable particle positions.

Hereinafter, the (-) particle in layer 1 and (+) particle in layer 2 are designated as particles 1 and 2, respectively. In the calculation, all the particle sizes were set to 1000 nm (a_1 = a_2 = 500 nm), Z_1 = −10000, and Z_2 = +10000. It is assumed that the closest distance δ between any two particles is 1 nm; namely, when two particles are in contact, $r = r_0 = 2a_1 + \delta$. The distances between the centres of the (+) particle and each of the seven (-) particles are expressed geometrically using θ, and the sum of interaction energies is donated as $U(\theta)$. Figure 8(c) is a plot of $U(\theta)$ / $k_{\mathrm{B}}T$ *vs.* θ calculated for various values of C_{s}, ranging from 2 μM (the impurity level in pure water) to 1500 μM. This indicates that the (+) particle is the most stable at θ = 1.23; i.e., when it is located in the centre of an equilateral triangle of the nearest-neighbour particles in layer 1. Figure 8(d) shows the force F acting on the (+) particle as a function of θ, which was calculated from $F = -(1/r_0)\, dU/d\theta$.

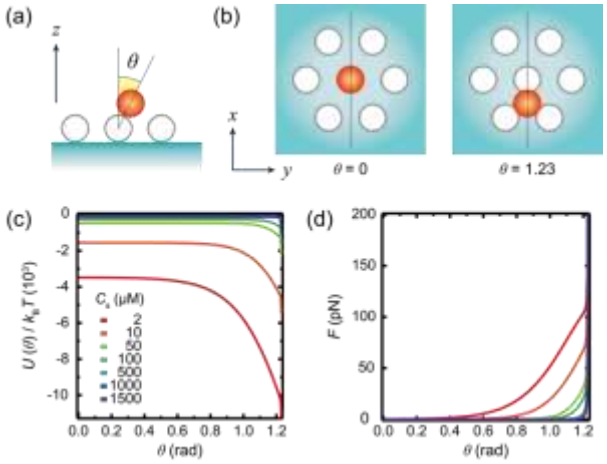

Fig. 8 Definition of the bond angle θ; (a) Side view: θ is the angle between the vertical line and the line segment connecting the centres of the particles in layers 1 and 2, (b) top views: θ = 0 when the particle in layer 2 is on top of the particle in layer 1. (c) Total interaction potential $U(\theta)$ between the (+) particle and seven (-) particles in the triangular lattice in layer 1 as a function of θ for various values of C_{s}. (d) Force F acting on the (+) particle obtained from $U(\theta)$. The colors of the curves represent the same C_{s} values as in (c).

3.5.2 Interaction between the (–) particle in layer 3 and the particles in the other two layers

We examined the conditions in which the particles in the three layers are arranged in a tetrahedral shape. The electrostatic forces acting on the (-) particle in layer 3 are shown schematically in Fig. 9(a). Each (+) particle in layer 2 exerts an electrostatic attraction (F_{pos}) on the (-) particle in layer 3. On the other hand, the three (-) particles in layer 1 cause electrostatic repulsion. When the vertical component of the repulsion from the single (-) particle is F_{neg}, the force exerted by the three particles in the triangular lattice is $3F_{\mathrm{neg}}$. The contribution of the

electrostatic interactions from particles other than these was neglected and all particle–particle interactions were assumed to be the Yukawa type.

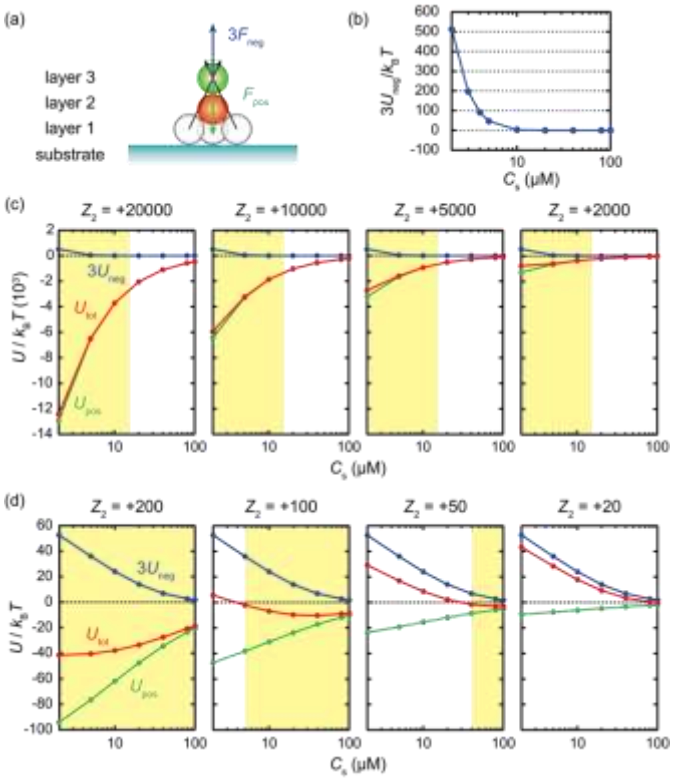

Fig. 9 (a) Illustration of the electrostatic forces acting on the particle in layer 3. (b) Interaction potential for the electrostatic repulsion by the three particles in layer 1, $3U_{neg}$ (d = 1000 nm, Z_1 = Z_3 = -10000). Interaction potential curves of the particle in layer 3 with various values of Z_2 for (c) the same conditions as in (b), and (d) d = 100 nm and Z_1 = Z_3 = –100. U_{pos} is the potential energy due to the (+) particle in layer 2, and $U_{tot} = 3U_{neg} + U_{pos}$. Regions shaded by yellow satisfy $3U_{neg} > k_BT$ and $|U_{tot}| > k_BT$.

The interaction potential energy of the particles arranged in a tetrahedron was calculated. d was set to 1000 nm for all particles and Z_1 = Z_3 = –10000. $3U_{neg}$ and U_{pos} were defined as the potential energies due to the forces $3F_{neg}$ and F_{pos}, respectively, and $U_{tot} = 3U_{neg} + U_{pos}$. A plot of $3U_{neg}$ *vs.* C_s. is shown in Fig. 9(b). Figure 9(c) shows plots of U_{tot}, $3U_{neg}$, and U_{pos} *vs.* C_s calculated for four different values of Z_2.

When the particles in layers 1 and 2 exist in an ideal position for tetrahedral arrangement, the following two conditions must be satisfied in order for the (-) particle in layer 3 to be located at the vertex of the tetrahedron: (i) The magnitude of U_{tot} must be greater than $1k_BT$, and (ii) the particle in layer 3 must be strongly repelled by the three particles in layer 1, that is, U_{neg} / k_BT > 1. Figure 9(c) shows in yellow the regions where both conditions (i) and (ii) are satisfied. These are met when C_s is sufficiently low (approximately 15.5 μM), showing a close correspondence with the experimental condition (20 μM). For comparison, the results for cases with d = 100 nm in shown in Fig. 9(d). Here, we chose Z_1, Z_2, and Z_3 so that the charge densities of the particles were equal to those of the case with d = 1000 nm. Unlike that case, the repulsion from the particles in layer 1 was strong enough to prevent the adsorption of the (-) particle of layer 3 onto the (+) particle. In particular, for $Z_2 \le 100$, low C_s conditions were rather unfavorable for making a regular stacking of layer 3.

3.6 Optical properties of the 2D diamond lattices

In this study, we fabricated a 2D diamond-like structure having three layers using colloidal particles. Here, we theoretically examined the optical properties of the 2D multilayer structure and a bulk diamond structure.

It is known that the bulk diamond lattice of colloidal particles with a sufficiently large refractive index has a perfect PBG, which allows for light confinement[1]. The perfect PBG is formed when the ratio of the refractive index of the particle, n_p, to that of the medium is greater than approximately 2[1]. For example, titania (rutile) particles have n_p ~ 2.8 in the visible light region[29] and therefore the diamond structure of titania particles in air has a perfect PBG. We calculated the photonic band diagram of the bulk diamond lattice by the plane wave expansion (PWE) method. Calculations were performed using the commercial software Opti FDTD (Optiwave Systems Inc., Ottawa, Canada). Dispersion of dielectric constant[29] was taken into account (Details are shown in SI1†). Figure 10(a) shows the photonic band structure of the 3D bulk diamond crystal of titania particles with d = 200 nm in air. The crystal had the full PBG in the frequency region 1.255 μm^{-1} to 1.334 μm^{-1}, which corresponded to the wavelength region of 750 nm to 797 nm.

Next, the optical properties of multilayered structures were examined by FDTD calculations. Details of the calculations are shown in SI2†. When the number of layers N = 4, the cage of the diamond lattice becomes a closed structure. Thus, 4-layer structures are often used as the smallest unit of the diamond lattice[4]. Calculations were performed for N = 3 and also for N = 4, 8, and 16. The models for the calculations are shown in Fig.10(b). Light is incident from a direction perpendicular to each layer ([111] direction). In all cases, lattices of titania particles of 200 nm in air were assumed. Figure 10(c) shows the reflection and transmission spectra calculated by the FDTD method. In Fig. 10(c), we also show the region of the full PBG of the 3D bulk diamond crystal and that of the PBG when incident from the [111] direction, i.e., a band gap at L point in Fig. 10(a). The spectra of the multilayers showed high reflectance (low transmittance) in the wavelength range of approximately 750-1000 nm, and it approached that of the bulk PBG with increasing N. Note that the structure with N = 4 showed about twice the reflectance of N = 3. As mentioned above, it was shown that the multilayered structures have the characteristics of photonic crystals.

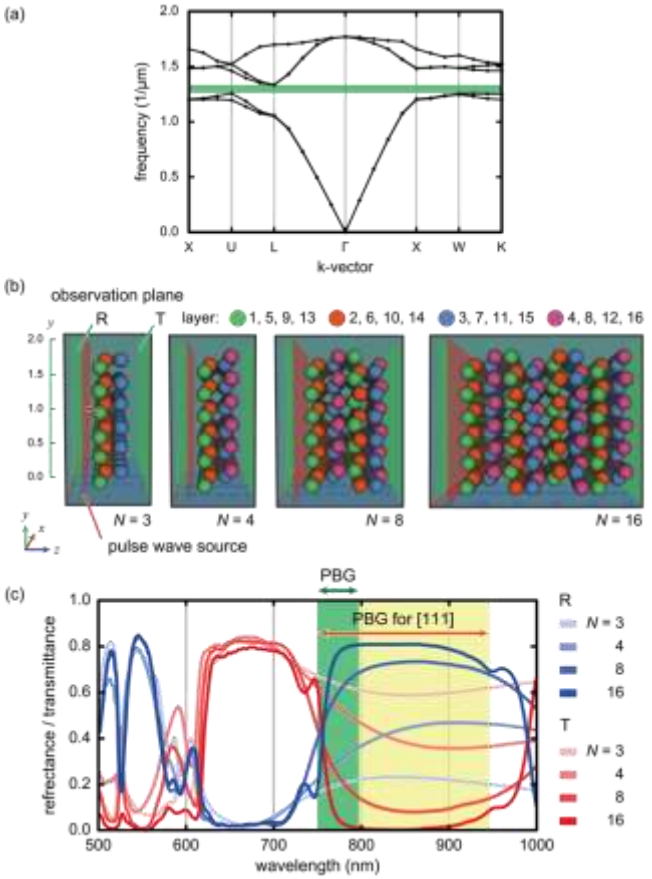

Fig.10 Calculated optical properties of diamond lattices. (a) The photonic band structure of the 3D bulk diamond crystal of titania particles with d = 200 nm in air. (b) Models used in the calculations; N is the number of layers. (c) Calculated reflection (R) and transmission (T) spectra for the 2D diamond lattices. The full PBG and PBG for incident light in [111] direction are also shown.

3.7 General discussion on the present methodology

Various ingenious studies have so far been reported on the construction of colloidal diamond crystals using submicron-sized particles[5-8]. In these studies, specific interactions are often introduced by complementary binding of DNA-modified particles. 3D diamond lattices have also been constructed by pre-fabricating tetrahedral clusters and exploiting anisotropic interactions between them[6-8].

One of the previous methods utilized colloidal alloys[6]. In binary colloids with a specific particle size ratio, a $MgCu_2$ superlattice is formed under appropriate mixing ratios. This superlattice is an interpenetrated structure of two types of crystals composed of a diamond lattice and a pyrochlore lattice. The diamond lattice is obtainable by removing the pyrochlore lattice from the superlattice. However, since there exist various crystalline phases other than the $MgCu_2$ structure in binary colloids and the difference in the free energy of each phase is not significantly large, it is not always possible to obtain only the desired structure. Ducrot et al.[6] constructed $MgCu_2$ superlattice of particles with d = 600-800 nm and preformed tetrahedral clusters of particles. The particles and clusters are both modified with DNA molecules complementary to each other. Selective interparticle attractions resulted in highly ordered $MgCu_2$ superlattice, leading to the formation of polycrystalline diamond structures with an area of more than 50 μm square.

He et al.[8] have recently reported a method for fabricating diamond structures by self-assembly of tetrahedral clusters as the building blocks, which were synthesized from particles approximately 1000 nm. Because of the anisotropic interactions similar to those of carbon atoms, they formed diamond lattices with excellent regularity and a thickness of 10-20 clusters.

Compared to these previous methods, our approach presented in this paper employs spherical particles with isotropic electrostatic interaction and has the advantage of easily fabricating large-area lattice structures and being applicable to a variety of materials and particle sizes. However, the resulted structures are currently limited to 2D, and they are more irregular than those obtained in the previous studies. As shown in Fig. 5(a), lattice defects of the crystal exist even in layer 1. Since these defects also affect the regularity of layers 2 and 3, it is necessary to further improve the crystallinity of layer 1. The possible causes of the crystal defects are as follows: (i) Before adsorption, particles form non-close-packed polycrystals due to sedimentation and concentration, and therefore have lattice defects originating from crystal grain boundaries. (ii) After adsorption, particles can be desorbed by flow in the process of washing excess non-adsorbed particles in the cell. Possible methods to reduce the defects include (i) unidirectional growth to fabricate a single crystal[22] and (ii) replacement of medium with a flow cell.

One of the challenges for the future is the construction of the lattice beyond the third layer: when viewed from the normal direction of each layer, the particles in the fourth layer must be located in the centre of the equilateral triangle created by the nearest three particles in layer 1. The electrostatic repulsion from the (+) particles in layer 2 may need to be strong enough to create this structure through electrostatic interaction. In this regard, it has been reported that diamond lattices of oppositely charged binary colloids are formed only when the Debye screening length is considerably larger than the particle size[16,17]; thus, smaller particles can be more favorable.

In addition to electrostatic interactions, a combination of other interactions can be useful. For example, depletion attraction due to soluble polymers, which is unaffected by particle charge, would be a candidate. We are currently conducting a detailed study by computer simulation.

4 Conclusions

This study demonstrates that a 2D diamond structure of micron-sized colloidal particles can be obtained by layer-by-layer electrostatic self-assembly. By adjusting the volume fraction of the dispersion and the magnitude of the electrostatic interactions between the particles, the interparticle distance of the crystal and the stacking position were controlled. For photonic applications, a diamond lattice with a higher refractive index ratio is desirable. The FDTD calculations show that the 2D diamond structures of titania particles have an absorption band in the wavelength range corresponding to the PBG of the 3D

bulk crystal. We are going to work on the fabrication of 2D diamond structures of particles with a higher refractive index. The result of the present study is expected to be useful for the construction of novel 2D photonic materials.

Author Contributions

MF conducted experiments, analyses, and potential calculations. AT supported experiments and TO assisted with potential calculations. HN and MF carried out calculations on optical properties. JY supervised the entire study and performed potential calculations.

Conflicts of interest

There are no conflicts to declare.

Acknowledgements

We would like to thank Professors Satoshi Uda and Jun Nozawa, Tohoku University, for their helpful discussion. We are grateful to Mr. Hiroyuki Miki, Nagoya City University, for his kind help on the data analysis. This research was funded by Grant-in-Aid for Scientific Research (17K04990 and 21K05008) from the Japan Society for the Promotion of Science. Part of this work was supported by the Japan Science and Technology Agency, "Establishment of University Fellowships towards the Creation of Science Technology Innovation".

Notes and references

1 K. M. Ho, C. T. Chan and C. M. Soukoulis, *Phys. Rev. Lett.*, 1990, **65**, 3152-3155.
2 K. Edagawa, S. Kanoko and M. Notomi, *Phys. Rev. Lett.,* 2008, **100**, 013901.
3 H. Yin, B. Dong, X. Liu, T. Zhan, L. Shi, J. Zi, and E. Yablonovitch, *Proc. Natl. Acad. Sci.,* 2012, **109**, 10798-10801.
4 T. Tajiri, S. Takahashi, C. A. M. Harteveld, Y. Arakawa, S. Iwamoto and W. L. Vos, *Phys. Rev. B,* 2020, **101**, 235303.
5 A. P. Hynninen, J. H. J. Thijssen, E. C. M. Vermolen, M. Dijkstra and A. van Blaaderen, *Nat. Mater.,* 2007, **6**, 202-205.
6 É. Ducrot, M. He, G.-R. Yi and D. J. Pine, *Nat. Mater.,* 2017, **16**, 652-657.
7 Y. Wang, I. C. Jenkins, J. T. McGinley, T. Sinno and J. C. Crocker, *Nat. Commun.,* 2017, **8**, 14173.
8 M. He, J.P. Gales, É. Ducrot, Z. Gong, G.-R. Yi, S. Sacanna and D. J. Pine, *Nature,* 2020, **585**, 524-529.
9 J. H. Moon and S. Yang, *Chem. Rev.*, 2010, **110**, 547-574.
10 F. Li, D. P. Josephson and A. Stein, *Angew. Chem. Int. Ed.,* 2011, **50**, 360-388.
11 N. Vogel, M. Retsch, C.-A. Fustin, A. del Campo and U. Jonas, *Chem. Rev.*, 2015, **115**, 6265-6311.
12 B. Li, D. Zhou and Y. Han, *Nat. Rev. Mater.*, 2016, **1**, 15011.
13 Z. Cai, Z. Li, S. Ravaine, M. He, Y. Song, Y. Yin, H. Zheng, J. Teng and A. Zhanga, *Chem. Soc. Rev.,* 2021, **50**, 5898-5951.
14 M. E. Leunissen, C. G. Christova, A.-P. Hynninen, C. P. Royall, A. I. Campbell, A. Imhof, M. Dijkstra, R. van Roij and A. van Blaaderen, *Nature,* 2005, **437**, 235-240.
15 T. Hueckel, G. M. Hocky, Palacci, J. Palacci, and S. Sacanna, *Nature,* 2020, **580**, 487-490.
16 A. M. Kalsin, M. Fialkowski, M. Paszewski, S. K. Smoukov, K. J. M. Bishop and B. A. Grzybowski, *Science,* 2006, **312**, 420-424.
17 K. J. M. Bishop, N. R. Chevalier and B. A. Grzybowski, *Phys. Chem. Lett.,* 2013, **4**, 1507-1511.
18 V. N. Manoharan, M. T. Elsesser and D. J. Pine, *Science,* 2003, **301**, 483-487.
19 E. Spruijt, H.E. Bakker, T. E. Kodger, J. Sprakel, M. A. C. Stuarta and J. van der Guchta, *Soft Matter*, 2011, **7**, 8281-8290.
20 N. B. Schade, M. C. Holmes-Cerfon, E. R. Chen, D. Aronzon, J. W. Collins, J. A. Fan, F. Capasso and V. N. Manoharan, *Phys. Rev. Lett.,* 2013, **110**, 148303.
21 H. Miki et al., *npj Microgravity,* 2023, DOI: 10.1038/s41526-023-00280-5.
22 Y. Aoyama, A. Toyotama, T. Okuzono and J. Yamanaka, *Langmuir,* 2019, **35**, 9194-9201.
23 Y. Nakamura, M. Okachi, A. Toyotama, T. Okuzono and J. Yamanaka, *Langmuir* 2015, **31**, 13303-13311.
24 T. Okuzono, K. Odai, T. Masuda, A. Toyotama and J. Yamanaka, *Phys. Rev. E*, 2016, **94**, 012609.
25 A. van Blaaderen and A. Vrij, *Langmuir*, 1992, **8**, 2921-2931.
26 W. B. Russel, D. A. Saville and W. R. Schowalter, Cambridge University Press, 1989, DOI: 10.1017/cbo9780511608810.
27 V. J. Anderson and H. N. W. Lekkerkerker, *Nature,* 2002, **416**, 811-815.
28 J. Yamanaka, T. Okuzono and A. Toyotama, Elsevier Inc., 2013, DOI: 10.1016/C2011-0-07715-3.
29 J. R. DeVore, *J. Opt. Soc. Am.*, 1951, **41**, 416-419.

